Influence of structural changes in a periodic antidot waveguide on the spin-wave spectra

J. W. Kłos,[1,*] D. Kumar,[2,*] M. Krawczyk,[1,†] and A. Barman[2,‡]

[1]*Faculty of Physics, Adam Mickiewicz University in Poznan, Umultowska 85, Poznań, 61-614, Poland*

[2]*Thematic Unit of Excellence on Nanodevice Technology, Department of Condensed Matter Physics and Material Sciences, S. N. Bose National Centre for Basic Sciences, Block JD, Sector III, Salt Lake, Kolkata 700 098, India*

(Received 30 June 2013; revised manuscript received 26 November 2013; published 7 January 2014)

We demonstrate that the magnonic band structure, including the band gap of a ferromagnetic antidot waveguide, can be significantly tuned by a relatively weak modulation of its structural parameters. We study the magnonic band structure in nanoscale spin-wave waveguides with periodically distributed small antidots along their central line by two independent computational methods, namely, a micromagnetic simulation and a plane-wave method. The calculations were performed with consideration of both the exchange and dipolar interactions. For the exchange dominated regime, we discuss, in details, the impact of the changes of the lattice constant, size, and shape of the antidots on the spin-wave spectra. We have shown that a precise choice of these parameters is crucial for achieving desired properties of antidot waveguides, i.e., a large group velocity and filtering properties due to existence of magnonic band gaps. We discuss different mechanisms of magnonic gap opening resulting from Bragg scattering or anticrossing of modes. We have shown that the dipolar interactions start to assert their role in the spin-wave spectrum when the waveguide is scaled up, but even for a period of few hundreds of nanometers, the magnonic band structure preserves qualitatively the properties found in the exchange dominating regime. The obtained results are important for future development of magnonic crystal based devices.

DOI: 10.1103/PhysRevB.89.014406 PACS number(s): 75.30.Ds, 75.75.−c, 75.78.Cd, 75.70.Ak

I. INTRODUCTION

The possibility for fabrication of metallic magnetic materials with nanoscale precision has opened the way for tailoring the dispersion of high-frequency spin waves (SWs). This can be done also with the use of magnonic crystals (MCs), which are magnetic counterparts of photonic crystals.[1,2] The first bicomponent MCs have been realized at nanoscale (a few hundred nanometers period) and the opening of magnonic gaps was proved experimentally.[3–5] Two-dimensional (2D) antidot lattices (ADL) formed by a periodic array of holes in a ferromagnetic film can be much easily fabricated than bicomponent structures. These systems have been intensively studied in recent years on length scales from micrometers down to few tens of nanometers.[6–11] In the larger scale, the inhomogeneity of the internal demagnetizing field is decisive for the formation of the magnonic band structure in ADL.[12,13] With decreasing period of ADL, the Brillouin zone (BZ) boundaries move to larger wave vectors and the exchange interactions at some point will start to play a primary role in the formation of a magnonic band structure and opening of magnonic band gaps.

Basic magnonic devices have already been demonstrated to be promising for technological applications[14–17] but the scaling down of magnonic elements to tens of nanometers in size and tens of gigahetz of operating frequencies are still a challenge. Recently, the spin-torque nano-oscillators were shown as a promising source of high frequency SWs.[18–20] To transmit the signal from the source, a waveguide needs to be properly designed. Thus a magnonic waveguide is an important component in most magnonic devices[14] and has been realized experimentally, so far, only for SWs in the frequency range up to few gigahertz.[8,21–26,33] To predict properties of magnonic devices at nanoscale, more basic research needs to be conducted. Therefore a theoretical investigation of the SW waveguides operating in the range of tens of gigahetz is a frontier field of research in magnetism.

The periodic waveguide gives the possibility to design selective leads that possess the filtering properties for transmitted SWs due to the presence of magnonic gaps. The position and the width of those gaps can be controlled by the structural parameters of the waveguides or by the bias magnetic field. It is also possible to design frequency dependent delay lines by exploiting the significant reduction of SW group velocity in the vicinity of magnonic gaps. The subject of periodic waveguides for SWs was extensively studied for the following geometries: (i) comblike structures and loop structures, where the SWs interference at the junctions in the brunched structures is crucial for a magnonic band gap opening.[27] (ii) Waveguides with periodically corrugated edges where the periodic change of the width is the main factor responsible for the generation of the magnonic band structure.[28] (iii) Ferromagnetic stripes where the periodicity of the magnetization is introduced by ion implantation[29] or (iv) a periodic bias magnetic field.[30] (v) SWs waveguides with periodicity introduced by a regular repetition of the bent sections where the bending induces a periodic anisotropy field.[31] Another class of periodic waveguides are systems with periodically placed antidots (holes),[32] which is not challenging for fabrication even with a resolution in the range of few nanometers.[11]

In this paper, we numerically investigate an antidot waveguide (ADW) made of permalloy (Py) with air holes (i.e., antidots) placed equidistantly along the wire in its center. The considered antidot waveguide having a width and period at the nanoscale will then operate in a frequency range of few tens of gigahertz. Here, we use two different computational techniques, a relatively fast plane-wave method[4,9] (PWM) to perform systematic studies and extensive micromagnetic simulations[28,30,34–36] (MSs) (with the aid of OOMMF software)[37] to verify the obtained results. Similar

ADW structures were already investigated in previous papers showing that ADWs have interesting properties that are relevant for technological applications.[32,38,39]

In Ref. 39, ADWs with comparable lattice periods and waveguide widths were considered (25% of the area occupied by the antidots). The influence of the static demagnetizing field and nonuniformity of the exchange field on the magnonic band structure in ADWs with various shapes of antidots was considered. In Ref. 32, it was shown that pinning of the magnetization at the edges of ADW can be an important factor that helps to open magnonic band gaps. Moreover, it was shown that antidots occupying as small as 5% of the ADW surface area are sufficient to open magnonic band gaps. In Ref. 38, the influence of the intrinsic and extrinsic mirror symmetry breaking on the magnonic band gaps in ADW with pinned magnetization at edges was investigated. It was shown that small deficiencies in the symmetry of the ADW structure can result in closing magnonic band gaps but it was also demonstrated that these band gaps can be reopened by an asymmetric external magnetic field. Nevertheless, the influence of thorough and systematic structural changes in ADW on magnonic band structure have not yet been considered towards the optimization of ADW design. Thus there is a need for comprehensive studies that will thoroughly explain the impact of different structural parameters on the SW spectrum of ADW and reveal interesting properties of the magnonic band structures. Such studies are also of crucial importance for experimental realizations of ADWs with magnonic band gaps and their practical applications. In this paper, we study the influence of antidot size, lattice period, shape, and size factor on the dispersion of SWs and magnonic band gaps in nanoscale ADW.

The paper is organized as follows. In Sec. II, we describe the structure of the ADW and calculation methods in brief. Subsequently, we explain the magnonic band structure in ADW and the influence of the structural changes, i.e., antidot size, lattice period, shape, and size factors, in Sec. III. Finally, we summarize our results and discuss the prospects of practical realizations. In Appendices A and B we describe in detail the plane-wave method and micromagnetic simulations, respectively.

II. THE WAVEGUIDE STRUCTURE AND THE CALCULATION METHODS

We study here the symmetric magnonic waveguides based on a one-dimensional (1D) antidot lattice structure shown in Fig. 1. It has the form of a thin (thickness 1 nm) and infinitely long permalloy ($Ni_{80}Fe_{20}$) stripe with a single row of square holes of side $s = 6$ nm disposed periodically along the central line. The stripe width and the lattice constant are fixed at 45 nm and $a = 15$ nm, respectively. The row of holes is placed at a distance of 19.5 nm from both top and bottom edges of the stripe. Thus the waveguide possesses an axis of mirror symmetry down the middle of the waveguide. Asymmetric waveguides show interesting changes to the SW band structure due to the loss of the mirror symmetry but this has been examined separately.[38] A bias magnetic field is applied along the stripe and it is strong enough to saturate the sample ($\mu_0 H_0 = 1$ T) and make the magnetization collinear and equal

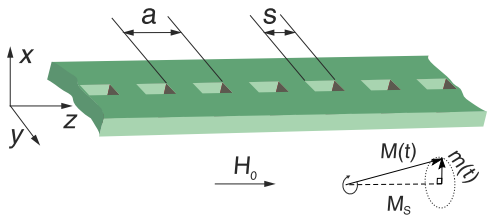

FIG. 1. (Color online) The structure of the antidot waveguide, where the row of the equidistant square holes was placed in its center. The size s and the distance between antidots (i.e., the period of the structure a) are 6 and 15 nm, respectively. The thickness of the waveguide is 1 nm. The sketch below the waveguide structure depicts the precession of magnetization around the direction of external magnetic field H_0.

to its saturation value even in the regions close to the sides of the waveguide and antidot edges. A saturation magnetization $M_s = 0.8 \times 10^6$ A/m, an exchange length $\lambda_{ex} = 5.69$ nm, and a gyromagnetic ratio $\gamma = 175.9$ GHz/T were assumed in the calculations.

The calculations of the magnonic band structure are performed with the PWM and the finite difference method based OOMMF. The PWM is implemented by a homegrown Fortran code and described in Appendix A.[40] MATLAB subroutines are written to analyze the data coming from OOMMF according to the algorithm presented in Fig. 6 in Appendix B.[41] Both methods solve the Landau-Lifshitz-Gilbert (LLG) equation:

$$\frac{\partial \mathbf{M}(\mathbf{r},t)}{\partial t} = \gamma \mu_0 \mathbf{M}(\mathbf{r},t) \times \mathbf{H}_{\text{eff}}(\mathbf{r},t) - \frac{\alpha}{M_s}\left(\mathbf{M}(\mathbf{r},t) \times \frac{\partial \mathbf{M}(\mathbf{r},t)}{\partial t}\right), \quad (1)$$

where $\mathbf{r}$ and t are position vector and time, respectively. μ_0 is the permeability of vacuum. The first term on the right-hand side is related to the torque inducing precession of the magnetization $\mathbf{M}$ and the second one describes the damping process (α denotes the damping constant). Damping is neglected in PWM calculations and included in MS ($\alpha = 0.0001$). The effective magnetic field $\mathbf{H}_{\text{eff}}$ here consists of the bias magnetic field $\mathbf{H}_0$, exchange field $\mathbf{H}_{\text{ex}} = \nabla \lambda_{\text{ex}}^2 \nabla \mathbf{M}$, and demagnetizing field $\mathbf{H}_{\text{dm}}$. For OOMMF calculations, the standard formula for dipole-dipole interaction in the latice of magnetic moments was used. In our PWM implementation, we use the Kaczer formula[50] for demagnetizing fields in planar periodic structures. Pinned dynamical components of the magnetization vector were assumed at Py/air interfaces in calculations with both methods.[32] The pinning in OOMMF was introduced by fixing the magnetization vector in all cells bordering the Py/air interfaces. (In MS, a discrete mesh size of $1.5 \times 1.5 \times 1$ nm^3 along X, Y, and Z axes, respectively, was used. The MS's were performed for 4 ns. In the PWM, we use 781, 1065, 1647 plane waves, depending on the value of the period a.) The boundary conditions for the dynamical component of magnetizations do not result from the Landau-Lifshitz equation. They can result from the presence of surface anisotropy (which depends on the physical and chemical state

of the surface) or from the so-called dipolar pinning.[42,43] Although we have limited our investigation to the case of pinned magnetization, the conclusions we draw will be still valid in systems with partially free magnetic moments on the external interfaces.[38]

The pinning at the edges of antidots forces the decay of the magnetization dynamics in the center of the ADW for small values of lattice constants a and relatively large antidot sizes s. By varying these parameters we can observe the gradual transition from the case of two weakly coupled periodic subwaveguides (formed by each of the two semi-isolated 19.5-nm-wide halves of the whole ADW) to the case of one waveguide (45-nm width, being the whole ADW) with small periodic perturbation (further discussion with numerical results will be presented in Sec. III B). In the PWM, the pinning is exactly at the edges of Py, whereas in MS the pinning was applied in a layer of finite thickness. This difference can slightly influence results obtained with both methods. The effect of magnetization pinning is seen in the profiles of SW dispersion relations shown in Figs. 2 and 3. Due to the small thickness of the ADW and relatively large ratio of the width to thickness of ADW, a uniform SW profile across the thickness is assumed. Both methods (PWM and MS) were already used in the calculations of the SW dynamics and proved to give correct results.[7,9,41]

III. THE INFLUENCE OF STRUCTURAL CHANGES IN THE ADW ON THE MAGNONIC BAND STRUCTURE

The dispersion relation, i.e., frequency as a function of the wave vector, $f(k)$, is a periodic function with a period equal to the reciprocal lattice vector $G = 2\pi/a$. This dispersion also has a mirror symmetry with respect to the point $k = 0$. Because of that, it is enough to show $f(k)$ only in the half of the first Brillouin zone (BZ) but for the purpose of clarity of analysis, we will present results in the full BZ.

A. The influence of antidot size

Figure 2 presents the SW spectra of ADW for three different sizes $s \times s$ of the square antidots: for $s = 4$, 6, and 8 nm. We kept the period of the ADW constant ($a =$ 20 nm). For a fixed period a, the increase of the antidot size makes the two subwaveguides (formed by halves of ADW) more isolated, because it reduces the crosstalk between magnetization dynamics in these two subwaveguides. It is noticeable both in the SW dispersion and in the profiles of the squared amplitudes of the dynamical magnetization in Fig. 2 (the profiles in Fig. 2 show the out-of-plane component of the magnetization vector). Let us compare the two lowest modes for $s = 4$ and 8 nm denoted in Fig. 2 by (a) and (b). For $s = 4$ nm, the lowest mode (a) is formed by strongly coupled SWs propagating in two subwaveguides. This mode, as the lowest one, has no nodal line in the center of ADW and therefore the SWs are allowed to penetrate in the areas between the antidots. The antidot with the larger size ($s = 8$ nm) can, however, successfully extinguish the SW dynamics in the ADW center. In this case ($s = 8$ nm), the modes (a) and (b) are almost degenerate with in-phase (a) and out-of-phase (b) SWs precession between two subwaveguides. Their amplitudes and

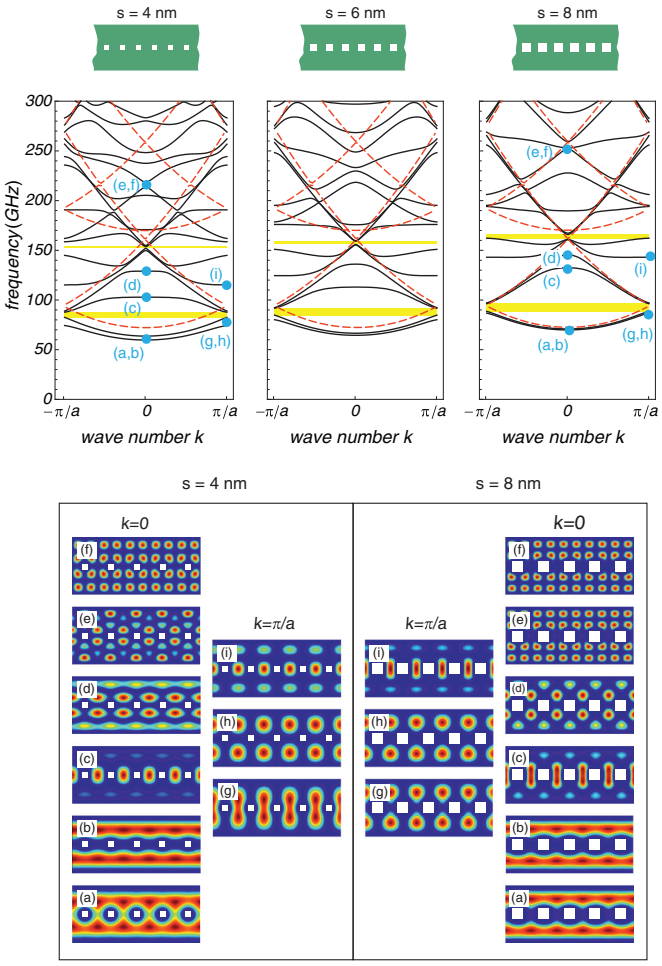

FIG. 2. (Color online) The dependence of size of antidots on SW spectra of ADW. The inset above the central part of the figure shows the system under investigation: 1-nm thick, 45-nm wide, infinitely long Py stripe with a periodic series of square antidots of size $s \times s$, where $s = 4$, 6, and 8 nm, disposed along the waveguide with a period of $a = 20$ nm. A bias magnetic field $\mu_0 H_0 = 1$ T is oriented along the waveguide. The row of antidots divides the waveguide into two subwaveguides. The coupling between subwaveguides is controlled by the size of antidots with small antidots resulting in strong coupling ($s = 4$ nm) and big antidots in weak coupling ($s = 8$ nm). Red dashed lines show the dispersion for a homogeneous waveguide of width $w =$ 19.5 nm with artificial folding-back of the dispersion to the first BZ. The colored maps present the squared amplitude of the out-of-plane component of dynamical magnetization for bands marked by letters from (a) to (i) in the SW spectra.

position of dispersion branches are almost the same. Mode (b) is, however, more robust to the changes in the antidot size. It is due to the fact that this mode has a nodal line in the center of the ADW, which leads to the decaying of the SW dynamics in the vicinity of the antidots row. As a result, the SWs mode (b) is weakly affected by the presence of the series of antidots placed in the middle of the structure. The comparison of the maps of mode (b) for $s = 4$ nm and for $s = 8$ nm does not show significant differences.

It is also visible that the shrinking of the antidot size, from 8 to 4 nm splits the levels of modes (a) and (b) gradually. The

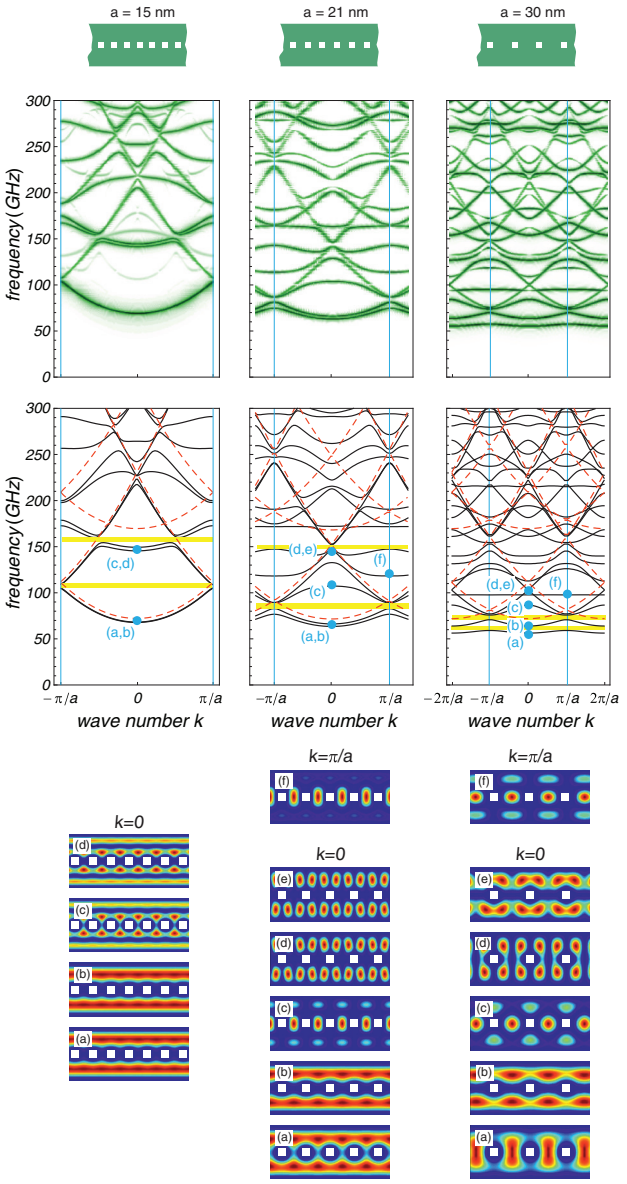

FIG. 3. (Color online) The dependence of SW spectra of ADW on the waveguide period. The size of the antidots is kept constant, $s = 6$ nm. The increase of the period (from $a = 15$ to 21 and 30 nm) leads to increase of the coupling between SWs in the subwavegudies. Note the change in location of the BZ edges marked by blue vertical lines. In the first row, schematic plots of the ADW are shown, in the second and third row, the dispersion of SWs calculated by micromagnetic simulations (OOMMF) and PWM are presented, respectively. Together with the PWM results, the dispersion for homogeneous waveguides of width $w = 19.5$ nm (for $a = 15$ and 21 nm) and $w = 45$ nm (for $a = 30$ nm) with artificial folding back of the dispersion to the first BZ is shown with dashed (red online) lines. The colored maps on the bottom of the figure show the squared amplitude of the out-of-plane component of magnetization calculated with PWM for points of the magnonic band structure labeled by (a)–(f).

difference between the frequencies of these modes becomes larger as the antidot size decreases. This increase of splitting between these modes can be attributed to an increase of dynamical coupling between SWs in subwaveguides, as is discussed in the next paragraph. One can notice also the small changes in the position for the two lowest modes in the frequency scale. The lowering of frequency of the modes can be attributed to the slight increase in the effective width of each subwaveguide with the reduction of the size of antidots.

The red dashed lines in the dispersion plots show the SW spectra for a plain waveguide of width of 19.5 nm,[44] which corresponds to the width of a single subwaveguide with $s = 6$ nm. The artificially introduced periodicity ($a = 20$ nm) folds the parabolic dispersion branches (typical for exchange dominated regime) to the first BZ. In the considered frequency range (0–300 GHz), two folded-back dispersion parabolas are visible related to the mode confinement and quantization across the waveguide. By comparing ADW spectra to the spectrum of the plain subwaveguide, the following features can be noticed. (i) The ADW dispersion branches, which mimic the spectrum of the plain subwaveguide [e.g., modes (a) and (b)] are confined mostly in the interior of the subwaveguides of ADW, whereas modes of ADW completely distorted from the parabolic shape [e.g., modes (c) and (d)] have amplitudes concentrated at the row of antidots. (ii) When the interaction between subwaveguides in ADW increases (for smaller antidot size), the distortion of paraboliclike dispersion branches is more significant. This effect is stronger for higher modes. For our system, already ADW modes related to the second parabola of plain subwaveguide are strongly perturbed. We can recognize at least two features of such distortion: the splitting between the modes being even and odd with respect to the ADW center [e.g., modes (a) and (b)], and the frequency downshift (stronger for modes originating from the second parabola) resulting from the increase of the effective width of the subwaveguides in ADW. For instance, modes (e) and (f) can be hardly identified as those related to the crossing of the folded arms of the second parabola in the BZ center (the modes have one nodal line in the center of each subwaveguide). They are significantly shifted down as the antidots are reduced.

Due to the periodicity in the system, the magnonic band gaps can be opened in the SW spectrum. If the periodicity can be regarded as a small perturbation in a plain waveguide, possible band gaps occur in three different scenarios: (i) at BZ edges, it happens for the lowest dispersion branch (originating from the first dispersion mode of the uniform waveguide), (ii) in the BZ center, as a result of the first self-crossing of the branches related to the same dispersion mode, after folding-back to the first BZ (only if there is no overlapping with higher modes, which can be supported by the sufficiently large value of the ratio period/width), and (iii) inside the BZ, being the effect of the anticrossing of branches related to different dispersion modes. Scenarios (i) and (ii) are related to the Bragg scattering for spin waves differing in wave number by $\Delta k = (2n)2\pi/a$ and $\Delta k = (2n+1)2\pi/a$, respectively, where n is an integer number. Such simple picture of the mechanisms can be used for very weak periodic modulation, where the dispersive branches in the system can be referred to as modes of the plain waveguide, and does not exhaust all possible mechanisms of band gap formation.[45–47] The magnonic gaps marked by yellow bars in Fig. 2 are related to the first and second scenario mentioned above. The gap generated by the anticrossing of branches related to the different dispersion parabolas of the plain subwaveguides (i.e., the third scenario)

can be observed in the first column in Fig. 3 (see the second gap for $a = 15$ nm). For the considered range of antidot sizes ($s = 4$, 6, and 8 nm), both gaps (the first and the second one) become slightly wider with an increase in the antidot size. However, introduction of much larger antidots (when $s \approx a$) will cancel the periodicity in the system and will lead to the gap closing. This behavior can be understood by considering two competing mechanisms. The gap will be wide when the periodicity is strong (large antidots with an interantidot distance comparable to the antidot sizes) and the crosstalks between subwaveguides are small (values of the ratio s/a close to 1 allows to separate subwaveguides). The first condition will enhance the Bragg scattering, the second one will reduce the splitting of the even and odd modes with respect to the ADW center.

B. The influence of lattice period

Figure 3 shows the variation in the magnonic spectra with the lattice constant ($a = 15$, 21, and 30 nm). We change the separation between the antidots keeping their size constant ($s = 6$ nm). The increase of lattice constant a contracts the size of the BZ. We decided not to change the range of the wave number k for successive values of a in Fig. 3. Therefore the dispersion plots for $a = 15$, 21, and 30 nm encompass: 1, $1\frac{1}{3}$, and 2 BZs, respectively. To discuss the impact of the lattice constant on the ADW spectrum, one has to include this additional factor. The reduction of the BZ size can affect the spectrum of the 1D periodic SW waveguide in two ways. (i) The SW spectrum contains more bands in the same frequency range. The edges of successive BZ appear more frequently in wave-vector domain and therefore the dispersion foldings at the BZ edges split the bands more often in frequency domain. (ii) The group velocity is reduced. If the spectrum is folded back multiple times, the number of bands reaching the BZ edge and center (where the group velocity drops to zero) increases. Both the Bragg scattering and self-crossing of bands leads to the band repulsion and their flattening.

Because of the much more complex evolution of the magnonic spectrum with changes in the lattice constant, it is more difficult to trace the variations in the origin of the band-gap width. The shrinking of the BZ (with the increase of a) changes the frequency position of the band gap opened at the BZ edges and can also result in opening or closing of gaps formed due to self-crossing or anticrossing of dispersion branches. Nevertheless, some characteristic features for this evolutions can be noticed. (i) The magnonic band gaps are shifted down in the frequency range. This is caused by the dense folding of the dispersion branches in the narrower BZ. The reasonably strong band overlapping, for larger values of a, can also close the band gaps in a higher frequency range (see Fig. 3 for $a = 30$ nm). (ii) There is no simple answer to what value of a is optimal for the existence of a wide magnonic band gap. The limits of very small and very large lattice constant (with a fixed antidot size) do not support the wide band gaps in the system. For short periods, the antidots start to overlap, which cancels the periodicity and makes two subwaveguides isolated (in terms of exchange interactions) and the band gap closes. In the limit of large lattice constants ($a \gg s$), the periodicity in the system can be treated as a small perturbation and, therefore, the Bragg scattering should be weak and it leads to a gradual band-gap closing. But the localized modes with flat bands appear in the low frequency spectra [see mode (a) in Fig. 3 for $a = 30$ nm] and the simple picture does not hold.

The increase of the lattice constant with the fixed size of the antidots makes the separation between the antidots larger. For $a \gg s$, ADW can not be treated as two weakly coupled subwaveguides. The data presented in the right column of Fig. 3 show that the considered system ($a = 30$ nm) is close to this limit. For even larger values of a, one may interpret the spectrum as a perturbation of the spectrum of the plain waveguide of width 45 nm (equals to the total width of ADW and is shown in the right column of Fig. 3 with dashed lines), rather than the spectra of two subwaveguides. Let us discuss how the increase in the ratio a/s affects the spatial distribution of modes (bottom row in Fig. 3). Two trends are evident: (i) the modes localized at the antidot row are shifted to the lower frequency range. Modes (c) and (f) for $a = 21$ and 30 nm have SW amplitudes localized between the antidots. With the increase of the period, the size of these areas extends, and the SWs confined in larger areas decrease their frequencies. (ii) The modes, even with respect to the ADW center, start to leak their amplitudes to the middle of ADW. For larger values of a, the pinning at the antidot edges is not sufficient to diminish the SW power at the center of the ADW even for the lowest modes. We can observe this process by analyzing the evolution of modes (a) and (b) while increasing the lattice constant. For $a = 15$ nm, it is almost impossible to distinguish between the profiles of the (a) and (b) modes. When $a = 21$ nm, the power from an even mode (a) starts to penetrate in the areas between the antidots. It leads to the coupling of excitation in the two subwaveguides and splits the dispersive branches of even (a) and odd (b) modes. The lowest mode of the large considered lattice constant $a = 30$ nm spreads its amplitude over the whole ADW width with maximum concentration in its center. Due to smoother spatial variation of the amplitude across the whole width of ADW (in comparison to the cases $a = 15$ or 21 nm), the frequency of this mode is lowered.

The second row in Fig. 3 presents the dispersions obtained from MS. The agreement with PWM is evident. Small discrepancies start to appear in the high-frequency range where the bands calculated using OOMMF are slightly shifted down. This can be attributed to finite cell sizes used in the finite difference method based solver. The maximum difference between the positions of the bands calculated in OOMMF and PWM reaches about 5% at the top of the presented spectra.

C. The influence of antidot shape

The effect of antidot shape on SW dispersion in ADW has been discussed in some detail for dipole dominated SWs[25,48] and exchange dominated SWs without pinning at Py/air interfaces.[39] Here, we revisit some of those findings for the completeness of this study. In order to make the systems of various antidot shapes comparable, we fixed the area of the antidots independent of their shape. We compared two basic antidot shapes: the square and the circular shapes. The results for $a = 15$ nm, $s = 6$ nm for square antidots, and radius of 3.38 nm for circular antidots are presented in Fig. 4. The SW

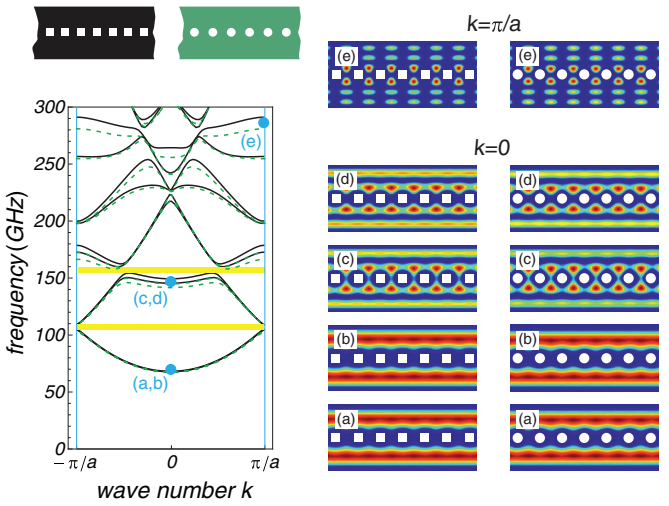

FIG. 4. (Color online) The SW spectra for the ADW with square (black solid line) and circular (green dashed lines) antidots. The lattice constant is fixed ($a = 15$ nm) and areas of square and circular antidots are the same (36 nm^2). The maps in the two columns on the right present the out-of-plane components of dynamical magnetization for selected modes in the center and the edge of the BZ for square and circular antidots, on the left and right, respectively.

spectra for these two antidot shapes do not differ significantly. The branches coinciding with the first dispersion parabola (cf. the red dashed line in the left column of the Fig. 3) almost overlap with each other. There is no discernible difference between modes (a) and (b) for both the ADWs with square and circular antidots. The levels associated with the second dispersion parabola [e.g., modes (c) and (d)] for the ADW with circular antidots are slightly lowered in reference to the corresponding modes of the ADW with square antidots. The differences in the profiles of (c) and (d) mode are also very subtle for two considered geometries. A more pronounced dissimilarity can be noticed for the modes localized at the row of antidots (e). For this case, almost the whole SW amplitude is focused in the vicinity of the antidots. Therefore this kind of excitation is relatively sensitive to the difference in shape of antidots, which is, in fact, a very small change in the geometry of the whole system. Similar effects were also found for other structures investigated in this paper, i.e., for lattice constants 21 and 30 nm and antidot sizes of 4 and 8 nm. Antidot geometry affects the exchange and demagnetizing field distribution around itself. Thus their periodicity in an ADW provides the periodic and inhomogeneous potential necessary for the Bragg scattering and the resultant characteristic SW spectrum. The demagnetizing field distribution is shown to play a more prominent role on larger length scales.[48] On the considered length scales, where we have exchange dominated SWs, the spectrum is affected only if the hole shape causes the exchange field distribution to change.[39] From the application point of view, perhaps the first direct magnonic band gap and related dispersive modes are the most important in the SW spectrum. Thus we find that, for exchange dominated SWs, even if minor periodic deformations of antidot shape occur during the fabrication of an ADW, its SW spectrum will remain practically unaffected as long as the exchange field distribution is unchanged.

D. The influence of size factor

For the ADW of width 45 nm discussed in the previous sections, the exchange interaction dominates over magnetostatic interactions. This results from the small values of dynamic demagnetizing fields in comparison to the exchange field for large values of wave numbers. Even the amplitudes of static demagnetizing field reach the values 0.1 T at the interfaces of Py/air perpendicular to the direction of the external filed, which are quite small in comparison to the value of external filed 1 T and to the width of the bands (taking $\gamma\mu_0 H_{\mathrm{dm}}$ for comparision). Therefore the SW dispersion manifests a pure exchange behavior with a paraboliclike trend visible even for wave numbers close to the BZ center [see, e.g., Fig. 4].

The models we use in the calculations include both kinds of interactions: exchange and dipolar. To observe a noticeable impact of dipolar interaction on the SW dispersion, one has to scale up the structure of ADW. We magnified the ADW structure with the square antidots presented in Fig. 4 by the factor of 6 (the width, thickness, antidot size, and lattice constant were all increased six times). For this structure in the first BZ, we observe a negative group velocity near the BZ center for the first two bands (Fig. 5), i.e., a feature characteristic for backward volume magnetostatic waves.[49] For lager values of the wave number, a quadratic dispersion

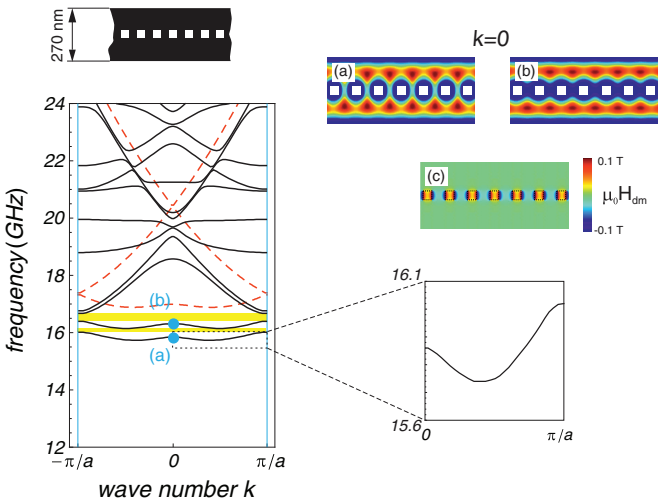

FIG. 5. (Color online) The PWM calculations of SW spectra for the ADW magnified by the factor of 6 in reference to the structure presented in Fig. 4 with square holes showing the crossover of exchange and dipolar effects related to the stronger manifestation of dipolar interactions. The structural parameters are the lattice constant, $a = 90$ nm, antidot size, $s = 36$ nm, and thickness and width, 6 and 270 nm, respectively. Red dashed lines show the dispersion for a homogeneous waveguide of width 135 nm [i.e., half of the total ADW width]. The maps (a) and (b) present the out-of-plane components of dynamical magnetization for two modes in the center of the BZ. (c) The map of the static demagnetizing field (its component along the waveguide, H_{dm}). The peaks of the static demagnetizing field are significantly smaller than the value of the external magnetic field $\mu_0 H_0 = 1$ T.

typical for exchange interaction begins to dominate. As a result, the two lowest dispersion branches have a minimum with a group velocity reaching zero away from the BZ center. The discussion of SW eigenmodes presented in the previous section has assumed the domination of exchange interactions. We have interpreted the magnonic band structure as an effect of crosstalks of two quasiparabolic dispersion relations related to two subwaveguides folded at the edges of the BZ. From Fig. 5, it is clear that even in a crossover of dipolar and exchange regime, this picture can be still valid and the spectrum presented in Fig. 5 preserves most of the features found for exchange dominated systems (cf. Figs. 2–4). We can also link the spectrum of the ADW [black lines in Fig. 5] to the spectra of homogeneous subwaveguides [red dashed lines] as well.

One of the important differences in comparison to exchange dominated systems is the increase of the strength of interactions between two subwaveguides. This effect is manifested by the stronger splitting of the levels of even [Fig. 5(a)] and odd [Fig. 5(b)] modes with respect to the ADW center. The increase of the coupling between these two SW excitations in different subwaveguides can be attributed to three factors: (i) to the enhancement of long-range dipolar interactions due to increased thickness of ADW, (ii) to the decrease of the band width [resulting from the large lattice constant and consequently smaller first BZ] and thus the relative increase of the role of nonuniformity of the static demagnetizing field [Fig. 5 (c)], and finally, (iii) to the increase of separation between antidots, thus the lowering frequency of quantized SWs between neighboring antidots. The considered regime of sizes [the width of the ADW presented in Fig. 5 equal to 270 nm] can be realized by a much broader spectrum of fabrication techniques, which make this system more interesting from the experimental point of view.

IV. CONCLUSIONS

We have presented an in-depth theoretical study of the impact of structural changes on the spin-wave spectrum of thin nanoscale magnonic waveguides with a row of antidots placed in their center. The influence of the antidot size and shape, distance between antidots, and the scale factor of antidot waveguides on the magnonic band structure and magnonic band gaps have been investigated. These studies allow for the identification of the main parameters and mechanisms that influence the width of magnonic band gaps in nanoscale ADW. Moreover, we have described the role of exchange and dipolar interactions in the formation of a magnonic band structure in a thin ADW with widths from tens to hundreds of nanometers. In summary, we have found that (1) the increase of antidot size in relation to the waveguide period makes the effective pinning in the center of the waveguide stronger. By controlling the strength of this pinning, one can affect the crosstalk between SWs propagating in two adjacent halves of the waveguide (subwaveguides). A gradual degeneracy of the (a) and (b) modes occurs as the antidot size increases.

(2) When the size of antidots is small enough, or the edge to edge distance between the neighboring antidots is large enough, the SWs localized on the periodic row of antidots are observed in a lower frequency range (together with the lowest dispersion branches for modes propagating in subwaveguides)—see, e.g., modes (c) and (i) in Fig. 2 [and also modes (c) and (f) in Fig. 3].

(3) The magnonic gaps are expected to open at the BZ edges or BZ center (Fig. 2). The gap can be opened for intermediate values of the wave number as well, where it is caused by the anticrossing of the bands originating from different transverse modes in homogeneous subwaveguides cf. modes (a), (b) and (c), (d) in the left panel in Fig. 2 [modes (a), (b) and (c), (d) differ in the number of horizontal nodal lines] and the second gap in this figure ($a = 15$ nm and $s = 6$ nm).

(4) When the waveguide period a is fixed then the existence of a magnonic band gap and change of its width and position is easier to analyze as a function of the antidot size s [Fig. 2], than for the opposite case, s fixed and a varied [Fig. 3]. It is because a change in a alters not only the strength of the periodicity but also affects the location of BZ edges. Nevertheless, the period of the ADW and its relation to the antidot size are important factors that influence magnonic band gaps and the group velocity of SW, thus, its proper choice will be crucial for application of nanoscale ADW in magnonics, to transmit or filter SW signals.

(5) The shape of the antidots does not affect the SW spectrum of exchange dominated SWs unless the exchange field distribution is altered. High frequency modes, which contain power close to the row of antidots show greater sensitivity towards changes in the shape of the antidots. Thus for modes from the low-frequency part of the spectra, the antidot shape is not an important parameter in nanoscale ADW.

(6) Enhancement of the size of an ADW increases the crosstalk between SWs propagating in two adjacent halves of the waveguide (subwaveguides) and the backward volume magnetostatic wave character of dispersion relation near BZ center for these SWs is found. However, still the main features of the magnonic band structure in the exchange dominating systems are preserved.

Thus we have shown that SW waveguides based on thin ferromagnetic stripes with a single row of periodically spaced antidots in nanoscale are promising for magnonic applications in frequencies from few to tens of gigahertz. Only a single row of antidots offer enough room for manipulation of the SW spectra to design single mode waveguides or waveguides with filtering properties due to existence of magnonic band gaps. The insensitivity of the main part of the magnonic spectra on the detailed shape of antidots, promises a possibility for fabrication of high frequency magnonic waveguides with the current technology.

ACKNOWLEDGMENTS

We acknowledge the financial support from the Department of Science and Technology, Government of India [Grant Nos. INT/EC/CMS (24/233552)], Department of Information Technology, Government of India [Grant No. 1(7)/2010/M&C], National Science Center of Poland (Project DEC-2-12/07/E/ST3/00538), and the European Community's FP7/2007-2013 [Grant Agreement Nos. 233552 (DYNAMAG)]. D.K. would like to acknowledge financial support from CSIR - Senior Research Fellowship [File ID: 09/575/(0090)/2011 EMR-I].

APPENDIX A: PWM - THE EIGENVALUE PROBLEM FOR LINEARIZED LANDAU-LIFSHITZ EQUATION

We considered the Landau-Lifshitz equation (1) in the linear approximation. We take into account the magnetization dynamics in the form of harmonic time precession of the magnetization with the angular frequency ω, expressed by the dynamical components of magnetization vector: $m_x(\mathbf{r},t) = m_x(\mathbf{r})e^{i\omega t}$ and $m_y(\mathbf{r},t) = m_y(\mathbf{r})e^{i\omega t}$. The dynamics of magnetization in the direction of external field is neglected, i.e., we assume $M_z(\mathbf{r},t) \approx M_s$. As a result, the linearized Landau-Lifshitz equations have a form of two linear differential equations for the precession amplitudes: $m_x(\mathbf{r})$ and $m_y(\mathbf{r})$. The amplitudes $m_x(\mathbf{r})$ and $m_y(\mathbf{r})$ can be transformed to the reciprocal space with the use of Bloch theorem. This allows to convert the linearized Landau-Lifshitz equations into the algebraic eigenvalue problem:

$$\begin{pmatrix} \{m_x(\mathbf{G})\} \\ \{m_y(\mathbf{G})\} \end{pmatrix} \hat{M} = \frac{i\omega}{\gamma\mu_0 H_0} \begin{pmatrix} \{m_x(\mathbf{G})\} \\ \{m_y(\mathbf{G})\} \end{pmatrix} \tag{A1}$$

by Fourier transformation of material parameters (M_s, λ_{ex}) and the periodic factor of Bloch functions, where $\{m_x(\mathbf{G})\}$ and $\{m_y(\mathbf{G})\}$ denote the vectors with the set of Fourier coefficients for periodic parts of Bloch functions. The matrix $\hat{M}$ of the eigenvalue problem can be written in a block-matrix form:

$$\hat{M} = \begin{pmatrix} \hat{M}^{xx} & \hat{M}^{xy} \\ \hat{M}^{yx} & \hat{M}^{yy} \end{pmatrix}. \tag{A2}$$

The submatrices in (A2) are defined as follows:

$$\hat{M}^{xx}_{ij} = -\hat{M}^{yy}_{ij} = -i\frac{k_y + G_{y,j}}{H_0|\mathbf{k}+\mathbf{G}_j|} S(\mathbf{k}+\mathbf{G}_j) M_s(\mathbf{G}_i - \mathbf{G}_j), \tag{A3}$$

$$\begin{aligned} \hat{M}^{xy}_{ij} = {} & \delta_{ij} \\ & + \sum_l \frac{(\mathbf{k}+\mathbf{G}_j)\cdot(\mathbf{k}+\mathbf{G}_l)}{H_0} l^2_{ex}(\mathbf{G}_l - \mathbf{G}_j) M_s(\mathbf{G}_i - \mathbf{G}_l) \\ & + \frac{(k_y + G_{y,j})^2}{H_0|\mathbf{k}+\mathbf{G}_j|^2}[1 - C(\mathbf{k}+\mathbf{G}_j, x)] M_s(\mathbf{G}_i - \mathbf{G}_j) \\ & - \frac{(G_{z,i} - G_{z,j})^2}{H_0|\mathbf{G}_i - \mathbf{G}_j|^2} M_s(\mathbf{G}_i - \mathbf{G}_j)[1 - C(\mathbf{G}_i - \mathbf{G}_j, x)], \end{aligned} \tag{A4}$$

$$\begin{aligned} \hat{M}^{yx}_{ij} = {} & -\delta_{ij} \\ & - \sum_l \frac{(\mathbf{k}+\mathbf{G}_j)\cdot(\mathbf{k}+\mathbf{G}_l)}{H_0} l^2_{ex}(\mathbf{G}_l - \mathbf{G}_j) M_s(\mathbf{G}_i - \mathbf{G}_l) \\ & - \frac{1}{H_0} C(\mathbf{k}+\mathbf{G}_j, x) M_s(\mathbf{G}_i - \mathbf{G}_j) \\ & + \frac{(G_{z,i} - G_{z,j})^2}{H_0|\mathbf{G}_i - \mathbf{G}_j|^2} M_s(\mathbf{G}_i - \mathbf{G}_j)[1 - C(\mathbf{G}_i - \mathbf{G}_j, x)], \end{aligned} \tag{A5}$$

where indexes i,j,l of reciprocal lattice vectors $\mathbf{G}_i$ are integers. $M_s(\mathbf{G}_i)$ and $l^2_{ex}(\mathbf{G}_i)$ are Fourier coefficients of the saturation magnetization and exchange constant, respectively. The additional functions used in the equations above are defined as follows:

$$\begin{aligned} S(\mathbf{k},x) &= \sinh(|\mathbf{k}|x)e^{-|\mathbf{k}|d/2}, \\ C(\mathbf{k},x) &= \cosh(|\mathbf{k}|x)e^{-|\mathbf{k}|d/2}, \end{aligned} \tag{A6}$$

where d denotes the MAW thickness.

In order to use PWM for 1D structure of ADW we have to make the structure artificially periodic along the direction perpendicular to the waveguide axis. We make advantage of the supercell method, which exploits the fact that the properties of the confined system (in our case, the ADW of finite width) are equivalent to the properties of the set of its noninteracting copies. In Eqs. (A3)–(A5), we have already used two-dimensional wave vectors $\mathbf{k}$ and reciprocal lattice vectors $\mathbf{G}$ in the (y, z) space, which refers to the infinite sequence of parallel ADW separated by artificial material.[32] Calculations are performed for y component of the wave vector equal 0, i.e., the direction of propagation of SWs is limited to the ADW axis.

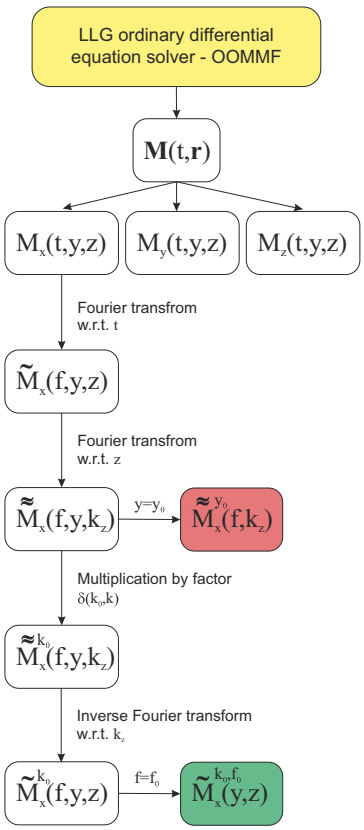

FIG. 6. (Color online) The computational scheme leading to dispersion relation $\tilde{M}^{y_0}_x(f,k_z)$ (red box) and spatial distribution of out-of-plane component of dynamical magnetizations for the selected eigenmode (k_0, f_0), $\tilde{M}^{k_0,f_0}_x(y,z)$ (green box) based on MS. f is a frequency of SW.

APPENDIX B: COMPUTATION OF DISPERSION RELATION AND MODES PROFILES WITH MICROMAGNETIC SIMULATIONS

The micromagnetic simulations were performed using OOMMF package. The calculation of dispersion relation is done in two stages: (i) simulation of magnetization dynamics in real space and time and (ii) multidomain Fourier transformation to obtain SW energy spectral density in frequency and wave-vector domains.[41] If the BZ extent is $2\pi/a$, then a mask $\delta(2n\pi/a \pm k_0)$ (where n is an integer) can be used such that an inverse Fourier transform (with respect to k_z) yields the SW mode profile corresponding to a given ordered pair (k_0, f_0).[39] The flowchart in Fig. 6 summarizes this procedure.

*These authors contributed equally to this work.
†krawczyk@amu.edu.pl
‡abarman@bose.res.in

[1] S. A. Nikitov, Ph. Tailhades, and C. S. Tsai, J. Magn. Magn. Mater. **236**, 320 (2001).
[2] H. Puszkarski and M. Krawczyk, Solid State Phenom. **94**, 125 (2003).
[3] Z.-K. Wang, V. Li Zhang, H. S. Lim, S. C. Ng, M. Hau. Kuok, S. Jain, and A. O. Adeyeye, ACS Nano **4**, 643 (2010).
[4] S. Tacchi, G. Duerr, J. W. Klos, M. Madami, S. Neusser, G. Gubbiotti, G. Carlotti, M. Krawczyk, and D. Grundler, Phys. Rev. Lett. **109**, 137202 (2012).
[5] M. Krawczyk, S. Mamica, M. Mruczkiewicz, J. W. Klos, S. Tacchi, M. Madami, G. Gubbiotti, G. Duerr, and D. Grundler, J. Phys. D: Appl. Phys. **46**, 495003 (2013).
[6] M. J. Pechan, Ch. Yu, R. L. Compton, J. P. Park, and P. A. Crowell, J. Appl. Phys. **97**, 10J903 (2005).
[7] S. Neusser, H. G. Bauer, G. Duerr, R. Huber, S. Mamica, G. Woltersdorf, M. Krawczyk, C. H. Back, and D. Grundler, Phys. Rev. B **84**, 184411 (2011).
[8] S. Neusser, G. Durr, H. G. Bauer, S. Tacchi, M. Madami, G. Woltersdorf, G. Gubbiotti, C. H. Back, and D. Grundler, Phys. Rev. Lett. **105**, 067208 (2010).
[9] S. Tacchi, B. Botters, M. Madami, J. W. Kłos, M. L. Sokolovskyy, M. Krawczyk, G. Gubbiotti, G. Carlotti, A. O. Adeyeye, S. Neusser, and D. Grundler, Phys. Rev. B **86**, 014417 (2012).
[10] C.-L. Hu, R. Magaraggia, H.-Y. Yuan, C. S. Chang, M. Kostylev, D. Tripathy, A. O. Adeyeye, and R. L. Stamps, Appl. Phys. Lett. **98**, 262508 (2011).
[11] R. Mandal, S. Saha, D. Kumar, S. Barman, S. Pal, K. Das, A. K. Raychaudhuri, Y. Fukuma, Y. Otani, and A. Barman, ACS Nano **6**, 3397 (2012).
[12] R. Zivieri *et al.*, Phys. Rev. B **85**, 012403 (2012).
[13] R. Zivieri, Solid State Phys. **63**, 151 (2012).
[14] V. V. Kruglyak, S. O. Demokritov, and D. Grundler, J. Phys. D: Appl. Phys. **43**, 264001 (2010).
[15] A. A. Serga, A. V. Chumak, and B. Hillebrands, J. Phys. D: Appl. Phys **43**, 264002 (2010).
[16] A. Khitun, J. Appl. Phys. **111**, 054307 (2012).
[17] *Magnonics: From Fundamentals to Applications*, edited by S. O. Demokritov and A. N. Slavin (Springer, Heidelberg, 2013).
[18] S. Bonetti, P. Muduli, F. Mancoff, and J. Akerman, Appl. Phys. Lett. **94**, 102507 (2009).
[19] O. Prokopenko, E. Bankowski, T. Meitzler, V. Tiberkevich, and A. Slavin, IEEE Magnetic Letters **2**, 3000104 (2011).
[20] M. Madami, S. Bonetti, G. Consolo, S. Tacchi, G. Carlotti, G. Gubbiotti, F. B. Mancoff, M. A. Yar, and J. Akerman, Nat. Nanotechnol. **28**, 635 (2011).
[21] A. Kozhanov, D. Ouellette, Z. Griffith, M. Rodwell, A. P. Jacob, D. W. Lee, S. X. Wang, and S. J. Allen, Appl. Phys. Lett. **94**, 012505 (2009).
[22] V. E. Demidov, M. P. Kostylev, K. Rott, J. Münchenberger, G. Reiss, and S. O. Demokritov, Appl. Phys. Lett. **99**, 082507 (2011).
[23] P. Clausen, K. Vogt, H. Schultheiss, S. Schäfer, B. Obry, G. Wolf, P. Pirro, B. Leven, and B. Hillebrands, Appl. Phys. Lett. **99**, 162505 (2011).
[24] G. Duerr, K. Thurner, J. Topp, R. Huber, and D. Grundler, Phys. Rev. Lett. **108**, 227202 (2012).
[25] S. Mamica, M. Krawczyk, and J. W. Kłos, Adv. Condens. Matter Phys. **2012**, 161387 (2012).
[26] C. Bilzer, T. Devolder, P. Crozat, C. Chappert, S. Cardoso, and P. P. Freitas, J. Appl. Phys. **101**, 074505 (2007).
[27] H. Al-Wahsh, A. Akjouj, B. Djafari-Rouhani, and L. Dobrzynski, Surf. Sci. Rep. **66**, 29 (2011).
[28] S.-K. Kim, J. Phys. D: Appl. Phys. **43**, 264004 (2010).
[29] B. Obry, P. Pirro, T. Bracher, A. V. Chumak, J. Osten, F. Ciubotaru, A. A. Serga, J. Fassbender, and B. Hillebrands, Appl. Phys. Lett. **102**, 202403 (2013).
[30] L. Bai, M. Kohda, and J. Nitta, Appl. Phys. Lett. **98**, 172508 (2011).
[31] V. S. Tkachenko, A. N. Kuchko, M. Dvornik, and V. V. Kruglyak, Appl. Phys. Lett. **101**, 152402 (2012).
[32] J. W. Kłos, D. Kumar, J. Romero-Vivas, H. Fangohr, M. Franchin, M. Krawczyk, and A. Barman, Phys. Rev. B **86**, 184433 (2012).
[33] V. Vlaminck and M. Bailleul, Phys. Rev. B **81**, 014425 (2010).
[34] K.-S. Lee, D.-S. Han, and S.-K. Kim, Phys. Rev. Lett. **102**, 127202 (2009).
[35] F. S. Ma, H. S. Lim, Z. K. Wang, S. N. Piramanayagam, S. C. Ng, and M. H. Kuok, Appl. Phys. Lett. **98**, 153107 (2011).
[36] Q. Wang, Z. Zhong, L. Jin, X. Tang, F. Bai, H. Zhang, and G. S. D. Beach, J. Magn. Magn. Matt. **340**, 23 (2013).
[37] M. Donahue and D. G. Porter, OOMMF Users guide, Version 1.0, Interagency Report NISTIR 6376 (NIST, Gaithersburg, 1999) at http://math.nist.gov/oommf/.
[38] J. W. Kłos, D. Kumar, M. Krawczyk, and A. Barman, Sci. Rep. **3**, 2444 (2013).
[39] D. Kumar, P. Sabareesan, W. Wang, H. Fangohr, and A. Barman, J. Appl. Phys. **114**, 023910 (2013).
[40] M. Krawczyk and H. Puszkarski, Phys. Rev. B **77**, 054437 (2008).
[41] D. Kumar, O. Dmytriiev, S. Ponraj, and A. Barman, J. Phys. D: Appl. Phys. **45**, 015001 (2012).
[42] K. Yu. Guslienko and A. N. Slavin, Phys. Rev. B **72**, 014463 (2005).
[43] G. T. Rado and J. R. Weertman, J. Phys. Chem. Solids **11**, 315 (1959).
[44] G. Venkat, D. Kumar, M. Franchin, O. Dmytriiev, M. Mruczkiewicz, H. Fangohr, A. Barman, M. Krawczyk, and A. Prabhakar, IEEE Trans. Mag. **49**, 524 (2013).

[45]J. Li, L. Zhou, C. T. Chan, and P. Sheng, Phys. Rev. Lett. **90**, 083901 (2003).
[46]C. Croenne, E. J. S. Lee, H. Hu, and J. H. Page, AIP Advances **1**, 041401 (2011).
[47]N. I. Polushkin, J. Appl. Phys. **114**, 033908 (2013).
[48]J. W. Kłos, M. L. Sokolovskyy, S. Mamica, and M. Krawczyk, J. Appl. Phys. **111**, 123910 (2012).
[49]D. D. Stancil and A. Prabhakar, *Spin Waves. Theory and Applications* (Springer, New York, 2009).
[50]J. Kaczer and L. Murtinova, Phys. Status Solidi A **23**, 79 (1974).